International Journal of Computational Research in Science and Technology
E-ISSN: 3108-0871, Volume 2 Issue 5
Sep-Oct 2026, PP 01-13

Microwave Sensor-Based Systems for Real-Time Detection of Microplastics in Water: A Review of Resonator Sensing, Microfluidic Integration, Machine Learning and Portable System Design

Prajyot Prakash Vishwasrao, Professor S. B. Bhosale
Dept. of Computer Engineering,
Jaihind collage of Engineering, Pune, India

Abstract. Microplastics (<5 mm) are now found in oceans, rivers, drinking water and human blood, yet routine monitoring is limited because reference methods such as Fourier-transform infrared (FTIR) and Raman spectroscopy are laboratory-bound, slow and costly. Microwave resonator sensing offers a low-cost, non-optical alternative: the large permittivity contrast between water (~80) and common polymers (~2–3.5) means suspended particles shift a planar resonator's resonance frequency, quality factor and transmission/reflection response. This narrative review covers sensing theory, resonator design, microfluidic sample handling, machine-learning interpretation (K-nearest neighbours, convolutional neural networks) and portable, wireless integration. Reviewed studies report resonance shifts of ~100 to >500 MHz, a theoretical resolution of ~100 ppm, a limit of detection of 48.72 ng/mL (microfluidic-CNN seawater system), response times below 250 ms, and prediction accuracies of 96–98 % within ±0.01 mg/mL. However, most studies use few polymers, filtered or artificial matrices, laboratory network analysers, non-standard concentration units and random data splits, and few address temperature or salinity compensation or long-term field operation; the seawater study's quoted detection limit and tolerance also need independent confirmation. We contribute a comparative analysis of representative studies, a conceptual architecture for field-deployable, IoT-connected monitoring, and a prioritised research agenda.

Keywords: Microplastics, Microwave Resonator, Dielectric Sensing, Microfluidics, Machine Learning, Convolutional Neural Network, Internet of Things

I. Introduction

Microplastics, defined as plastic particles smaller than 5 mm, have become a pervasive environmental contaminant. Global plastic production continues to outpace recycling, and much of the waste ends up in the environment [2]. Microplastics were reported in marine waters more than two decades ago [1] and have since been found in food and drinking water [3] and in human blood [4]. Their persistence and their potential effects on aquatic life and human health make quantitative monitoring necessary for risk assessment and mitigation.

Established analytical methods identify polymer chemistry reliably. These include Fourier-transform infrared (FTIR) spectroscopy [6], Raman imaging [7] and thermal-desorption gas chromatography–mass spectrometry [8]. Visual microscopy alone is unreliable for particles below about 200 µm [5]. Laboratory methods are accurate but centralised: they need bulky and costly

instruments, skilled operators, careful sample preparation and long analysis times [7], [10], [14]. They therefore cannot monitor rivers, treatment plants or coastal sites continuously, and most water bodies remain effectively unmonitored.

Microwave resonator sensing offers a complementary route. A planar resonator responds to the permittivity of the material in its fringing electric field. Common plastics have relative permittivity of about 2–3.5, while water is about 80, so the presence of plastic shifts the resonance frequency [10]. Malyuskin first demonstrated the feasibility of this approach for soil and water. He derived a linear relation between resonance shift and contaminant concentration and estimated a theoretical resolution of about 100 ppm [9]. Later work printed such sensors on ordinary circuit boards, integrated them with microfluidic channels [10]–[13], and recovered particle size and polymer type [10], [11]. Most recently, Hou et al. combined a microwave sensor with a convolutional neural network and a Bluetooth-enabled embedded reader for seawater [14].

Significant gaps remain. Detection limits reported for several laboratory prototypes still exceed the microplastic concentrations typical of freshwater [10]. Water strongly damps the resonance, reducing the quality factor by a factor of five or more [9]. Temperature, salinity and particle sedimentation disturb the measurement [10], [14]. Polymer discrimination, though promising (80–100% per class in one study [10]), has only been shown on small test sets of laboratory particles.

This paper reviews these developments in three strands: (i) sensing theory and resonator design, (ii) microfluidic sample handling and matrix effects, and (iii) machine-learning and embedded integration. It compares the reported performance of existing sensors, gives an analytical illustration of the expected permittivity change using effective-medium theory, and proposes a system architecture that addresses the weaknesses identified. The remainder of the paper is organised as follows: Section II gives the sensing theory, Section III reviews the state of the art, Section IV presents the proposed architecture, and Section V discusses challenges and conclusions.

II. Review Methodology

A focused narrative review was carried out on microwave and microwave-microfluidic microplastic sensing. The core evidence base comprises one journal article on a portable microfluidic convolutional neural network (CNN) seawater system [10], one IEEE Sensors Journal feasibility study on soil and water [6], and two graduate theses that describe the development of microwave-microfluidic sensors [11] and low-cost PCB resonators [13], together with related papers cited within them [7]–[9], [12]. The full texts were consulted, including the two appendices of the arXiv version of [6], the theory, simulation, fabrication and bench-measurement chapters of the 124-page dissertation [13], and the literature review and the environmental chapters of the 197-page thesis [11] (exploratory sensing, coupled-resonator sensing and single-particle classification). The final chapter of [11], which adapts the platform to measuring amylase in surgical drainage fluid, lies outside the scope of this review and is not used. The supplementary information of [10] (Figs. S1–S23 and Tables S3–S4) was not available to the reviewer, so values that the article takes from it are not checked here. Studies were included when they reported a microwave sensing approach for microplastics with a stated method and quantitative outcome. Values below are quoted as reported by the original authors; where a figure is read from a plot or recalculated by the reviewer, this is stated. No systematic database search or study count is reported, so the review is narrative rather than systematic, and results from different studies are not directly comparable because particle types, sizes, concentration units and matrices differ.

III. Sensing Principle and Resonator Design

1. Dielectric Contrast and Perturbation Theory

Microwave sensing differentiates materials by complex permittivity, $\varepsilon r = \varepsilon' - j\varepsilon''$, where ε' describes energy storage and ε'' dielectric loss [10]. Microplastics have real permittivity of roughly 2–3.5, whereas water is about 80, wet sediments 10–30 and

blood 50–60 [11]; at 5.5 GHz the contrast between water and Nylon 11 powder exceeds a factor of 20 in the real part and two orders of magnitude in loss tangent [6]. Introducing plastic into the resonator's sensitive region therefore lowers the effective permittivity and, in the simple perturbation picture, raises the resonance frequency of the loaded sensor (the sign of the shift actually reported differs between studies, as discussed below), while particle scattering and dilution of lossy water change the quality factor and amplitude [6], [10].

For small contaminant fractions (Vc < 0.1Vh), Malyuskin derived a linearised relation between the resonance shift and the contaminant volume fraction [6]:

$$\Delta f = \tfrac{1}{2} f0\ Vc\ (\varepsilon'h - \varepsilon'c) / (A + \varepsilon'h) \quad (1)$$

where f0 is the resonance of the uncontaminated host, ε′h and ε′c are the real permittivities of host and contaminant, and A is a geometry-dependent constant calibrated against a known sample (A = 55.8 for the PCB ring sensor in sand) [6]. The model agreed closely with measurements on Nylon 11 powder (50 µm–0.5 mm) in soil and implies a concentration resolution ΔVc = D·Δf/f0. Its authors conclude that, even for a quality factor of 2500 and receiver sensitivity of −100 dBm, the resolution in the linear regime is limited to about 100 ppm, and that improvement requires higher Q, low-noise amplification, non-linear detection or a smaller sensing volume [6].

Desbas approached the same problem with the Maxwell-Garnett effective-medium model, in which each particle polarises as a small dipole and the permittivity of the mixture is εeff = εhost[1 + 3fv(εinc − εhost)/(εinc + 2εhost)], where fv is the plastic volume fraction, εhost the permittivity of water (modelled with a Debye relaxation expression) and εinc that of the plastic [13]. Evaluated for a plastic permittivity of 2.25 and concentrations from 0 to 50 mg/mL, the model gives a steadily falling effective permittivity, and because the real part of the permittivity of water falls and its loss rises with frequency across the 1–6 GHz band used, the contrast depends on the operating frequency [13]. For small volume fractions a first-order expansion of this expression is linear in fv, so it agrees in form with the linear mixing rule of Eq. (1) (reviewer's observation).

The direction of the reported resonance shift is not uniform across the studies, and readers should not assume a single sign convention. Malyuskin's soil data and the simulations and measurements of ShafieiDarabi show the resonance moving upward as lower-permittivity plastic displaces the host, for example by about 0.4–0.5 MHz for 70 µm spheres at 107 particles/L against 4 MHz predicted by simulation [6], [11]. Hou et al., in contrast, report the resonance moving downward as concentration rises, with fitted slopes of −0.015, −0.014 and −0.0064 GHz per mg/mL in deionised water, artificial seawater and natural seawater [10], and Desbas observed both increases and decreases depending on the sensor design and particle size [13]. Possible causes such as particle aggregation, loading of the field by particles, the surfactant, or loss in the host are not investigated in any of the studies, so the sign convention should be stated explicitly whenever results are compared.

2. Resonator Topologies

The reviewed sensors are planar structures on low-loss printed circuit board (PCB) laminates. Malyuskin used a capacitively loaded square-ring resonator measured in reflection (scattering parameter S11, about 5.5 GHz, Q > 200 in air) whose electric field is concentrated in the capacitive gap [6]. Desbas simulated and fabricated two interdigital resonators (a simple and a capacitive design) with integrated microchannels and tested them from 1 to 6 GHz, placing particles in the highest-field regions identified by finite-element simulation in Ansys HFSS (High-Frequency Structure Simulator) [13]. ShafieiDarabi progressed from an exploratory microfluidic resonator to a coupled interdigital-capacitor and split-ring design that enhances sensitivity and allows size as well as concentration to be estimated [11], [12]. Hou et al. used a ring-type planar resonator measured in transmission (scattering parameter S21, simulated resonance near 2.8 GHz) and showed by HFSS simulation that dropping the sample on the annular gap in the upper part of the sensor gives the strongest and most regular response [10]. Related designs

include a complementary multi-split-ring microelectromechanical systems (MEMS) sensor with a micro-filter [7] and microwave cytometry with 3D electrodes for particle differentiation [9].

Design details differ in ways that matter for sensitivity. Malyuskin's sensor was printed on 1.6 mm FR4 (a glass-epoxy laminate) with ring dimension d = 12 mm, capacitor length Lc = 8 mm and a 40 mm feed line; widening the capacitive gap from 0.5 to 3 mm raised the simulated resonance from 5.40 to 6.10 GHz and cut the quality factor from 223 to about 90, so the gap trades Q against field penetration, and a 1.5 mm gap was used experimentally [6]. The sample sat in an acrylic holder of 12 × 12 × 10 mm and the response was recorded with a Keysight E8361C network analyser [6]. Desbas used a Rogers RT/duroid 5880 laminate (relative permittivity 2.2, loss tangent 0.0009, 1.6 mm), set the finger lengths, widths and spacings in HFSS, and refined them with a quasi-Newton optimiser in 0.1 mm steps until the sharpest resonance was obtained (simulated Q = 74.11) [13]. The fabricated sensor 1 resonated at 3.79 and 4.69 GHz against 4.07 and 4.98 GHz simulated, about 7 % lower at the first peak, which the author attributes to material and fabrication tolerances and contact imperfections [13].

In [11] the exploratory split-ring resonator (SRR) has a 1 mm capacitive gap, much larger than the 20–70 µm particles; the author notes that matching the gap to the particle dimension should raise sensitivity and proposes this as an improvement [11]. The later designs pair an interdigital capacitor (IDC) with an SRR in a tag-and-reader arrangement, and the single-particle platform energises two SRRs of different size through Wilkinson power dividers, giving simulated resonances at 1.227 and 2.617 GHz with a channel width matched to the SRR gap, so that each particle is probed at two frequencies [11]. For the seawater system, Hou et al. fabricated a ring-type resonator on Taconic TLX-8 laminate (relative permittivity 2.55, loss tangent 0.0019, 0.508 mm) by photolithography and chemical etching and modelled it with an equivalent circuit in Keysight Advanced Design System (ADS) as well as in HFSS; the simulated transmission minimum reached −48.5 dB near 2.8 GHz, with a second strongly excited mode at 3.2 GHz, and the sample-loaded resonances in the concentration experiments lie lower, at about 1.89–2.05 GHz (read from Fig. 2 of [10]).

3. Performance Metrics

Studies report the resonance frequency shift Δf, the amplitude of the transmission or reflection coefficient, the quality factor Q, and the percentage relative frequency shift (PRFS) [10]:

$$Q = fr / (fr{+}3dB - fr{-}3dB) \quad (2)$$

$$PRFS = (fr2 - fr1) / fr1 \times 100\ \% \quad (3)$$

$$LoD = K \cdot S0 / S \quad (4)$$

where LoD is the limit of detection, K = 3 is the confidence factor, S0 the standard deviation and S the calibration-curve slope [10]. Because the limit of detection depends on how S0 and S are obtained, it must be read together with the concentration range actually tested (Section IX).

Malyuskin also links resolution to the readout: the smallest detectable reflection change scales as $|\Delta S11| = 2|S11,min|(Q\Delta f/f0)2$, so a two-fold finer resolvable frequency step needs a four-fold finer amplitude sensitivity at constant Q, while the volumetric resolution is $\Delta Vc = D{\cdot}\Delta f/f0$, with D set by the permittivities and the geometry constant A [6]. Phase-locked-loop frequency synthesisers offer relative frequency steps of 10−5 to 10−8, which Malyuskin takes as evidence that tens-of-ppm resolution is possible from the frequency-tuning side, whereas the receiver sensitivity (−100 dBm in the worked example) sets the 100 ppm limit [6]. Hou et al. also report the loss tangent, $\tan\delta = \varepsilon''/\varepsilon'$, and derive capacitance and inductance from the measured admittance and impedance [10].

4. Reference Dielectric Data and Soil Measurements

Tables II and III collect the substrate, quality-factor and dielectric values reported in the studies. Malyuskin measured the dry host materials by free-space transmission at 5.5 GHz: topsoil (about 20 % organic matter) had a real permittivity of 4.70 and a loss tangent of 0.03, sandy soil (over 90 % sand) 5.60 and 0.007, and Nylon 11 powder 2.59 and 0.008, whereas fresh and 30 ppt salty water (literature values at 5.5 GHz) had 72.0 and 66.0 with loss tangents of 0.28 and 0.80 [6]. The plastic-to-host permittivity ratio is therefore about 2:1 in sand but nearly 28:1 in fresh water (calculated from these values). Because topsoil is more than four times as lossy as sand, the topsoil-loaded sensor had a Q of 92.4 against 259.8 for sand, which is higher than the 119.4 of the empty sensor [6]. In the soil experiments Nylon 11 (density 1.03 g/cm3, 50 µm–0.5 mm) was mixed at 0–500 parts per thousand (ppt, by volume, not parts per trillion) in 50 ppt steps, ten sub-samples per level, and the resonance sub-bands were averaged because particle position in the non-uniform field moved the resonance by up to ±3 MHz; shifts reached roughly 45–65 MHz at 500 ppt (read from Fig. 4c of [6]) and followed the linear model closely at low concentration [6].

IV. Microfluidic Integration and Sample Handling

Microplastic suspensions sediment, float and aggregate, so static drop measurements are poorly repeatable. Malyuskin observed that Nylon 11 forms emulsion-like mixtures and millimetre-scale clusters in tap water but surface clusters in salt water; partial loading of the resonator with a 1 mm × 9 mm water mini-channel was needed because full immersion reduced Q by a factor of five or more (Q ≈ 110 for tap water versus 218.7 for air), and shifts exceeding 140 MHz were seen depending on particle distribution [6]. Desbas integrated PCB microchannels with a pump and vector network analyser (VNA) bench to compare unloaded (water) and loaded (water with microplastics) states using plastic from sanded bottles and ground tyre rubber (< 300, 150 and 75 µm; 0.1, 0.5 and 1 %), but could not isolate the effect of salts, iron and other constituents of tap water [13].

In [13] the channel was cast in polydimethylsiloxane (PDMS, Sylgard 184) from a 3D-printed ceramic mould and placed above the resonator. The first-generation tests used a single ground-tyre particle of about 0.3 × 0.3 × 0.3 mm3, chosen because it passes through a syringe needle and is environmentally relevant; the second-generation suspensions were prepared from milled bottle plastic (polyethylene terephthalate, PET) and ground tyre rubber, size-sorted below 300, 150 and 75 µm [13]. Measurements were made in distilled water with a calibrated VNA using 801 points between 1 and 6 GHz, with a water baseline recorded before each injection [13]. The largest shifts occurred when particles sat in the highest-field region predicted by simulation, but concentration discrimination was weak: for particles below 300 µm the three concentrations differed by only about 6 MHz, whereas the step from water to plastic-laden water was 100–170 MHz; for sensor 2 the 0.5 % and 1 % responses converged at about 2.42 GHz (300–150 µm) and 2.30 GHz (below 150 µm), and the author notes that the response was not linear [13]. Sensor 2 gave almost no response through the microchannel and was re-tested with an open container on top of the resonator [13].

ShafieiDarabi's thesis moved from fixed microlitre samples in disposable holders to continuous flow, because small fixed volumes limit statistical robustness; with pre-filtering into size ranges, single-particle detection of 20–300 µm particles became possible [11]. Hou et al. compared a pool-type PDMS well with a tubular PDMS channel driven by a peristaltic pump: the tubular design gave tightly clustered replicate curves (10 repeats per concentration) with only small frequency shifts (≤ 0.1 GHz) relative to the bare sensor, and the response saturated above a 20 µL sample volume. Samples were ultrasonicated for 5 min and kept stirred [10].

The exploratory measurements in [11] used polyethylene (PE) microspheres of 20 and 70 µm suspended in 0.1 % Tween 20 surfactant, a temperature-controlled chamber (10–30 °C) and an analyser with 100 kHz resolution, so only shifts above about 0.1 MHz were treated as detectable; a replaceable reservoir was introduced because Tween 20 adhered to the chip and tubing.

The measured limit of detection was 106 particles/L for 70 µm spheres and 107 for 20 µm spheres, while simulation predicted 104 particles/L for 300 µm spheres at 10 °C [11]. Measured shifts were much smaller than simulated (about 0.5 MHz against 4 MHz for 70 µm spheres at 107 particles/L), and temperature changed the shift only slightly (0.39, 0.44 and 0.53 MHz at 10, 20 and 30 °C) because the high-permittivity background masks the contrast [11]. The coupled IDC–SRR design improved on this: 20 µm particles were detected at 105 particles/L, a hundred-fold lower than the exploratory result for the same size, and 20 and 70 µm particles were distinguished [11], [12]. In the continuous-flow platform the sample was driven at 50 µL/min and the resonance profile was read every 500 ms; particles of 250–300 µm needed about 20 s to cross the channel, yet 15 % (165–300 µm), 20 % (91–165 µm), 15 % (51–91 µm) and 35 % (16–29 µm) of particles were missed (reviewer's calculation from the reported counts of 20 reads per range), because particles can pass the sensing region between readings [11].

Matrix effects are decisive. Hou et al. report that rising temperature increases resonance frequency, Q and PRFS while higher salinity changes them in the opposite direction, so compensation is required, whereas pH between 4 and 10 had no notable effect; the natural seawater tested was pre-treated by multi-stage membrane filtration and density separation to remove algae, plankton and organic debris before microplastics were added [10]. The sensor therefore responded to controlled additions rather than to untreated seawater.

The carrier liquid matters as much as the particles. In [11] the same blue polyethylene microspheres (250–300 µm) were tested in deionised water, tap water and solutions of 0.1 M sodium chloride, 0.05 M urea, 0.01 M potassium nitrate and 0.01 M sodium nitrate, all with 0.1 % Tween 20; the measured permittivity of the carriers changed significantly even at these low solute concentrations, the average shifts were about 374 kHz for the small and 691 kHz for the large resonator, and the author concludes that each shift must be referenced to the baseline of the same carrier without particles [11]. Hou et al. also varied particle size and polymer [10]: polyvinyl chloride (PVC) powders of 2000, 1000 and 500 mesh (about 6.5, 13 and 25 µm) showed the same trend of falling resonance frequency and Q with concentration, with smaller particles dispersing more uniformly and scattering less, while polyethylene and polypropylene (PP) powders followed similar trends with weaker responses, PVC (the highest dielectric constant) giving the largest shift and PP the weakest. Suspensions at 3 mg/mL sedimented or floated, which limited the tested range to 0.5–2.5 mg/mL, and the polymer and size comparisons rest on supplementary Figs. S15–S18, which were not available for this review [10].

V. Machine Learning for Signal Interpretation

1. Why Machine Learning

Simple linear calibration of frequency against concentration became inaccurate once responses were nonlinear; Hou et al. found that the frequency shift increased non-uniformly with concentration and adopted deep learning for that reason [10]. ShafieiDarabi similarly trained a K-nearest-neighbours (KNN) classifier on raw sensor data to estimate particle size, concentration and polymer type from filtered environmental samples, covering a 20–300 µm size range [11].

2. CNN-Based Concentration Prediction

In [10], each transmission spectrum was reduced to 24 features: five frequency–amplitude pairs on each side of the resonance minimum, the minimum itself, and the Q and PRFS values. Twenty replicates per sample (4800 feature values in total) were split half for training and half for validation across five concentrations from 0.5 to 2.5 mg/mL of 6.5 µm PVC. The CNN predicted concentration within ±0.01 mg/mL with a reported 98 % correct rate on VNA data, and about 96 % on the portable hardware (ten training and ten validation groups per concentration) [10].

The article describes the network only through Fig. 3g, which shows an input layer, two convolution layers each followed by down-sampling, and two fully connected layers; the filter counts, learning settings and number of output classes are not given

in the main text, and the convergence curves are in supplementary Fig. S5 [10]. For the portable unit the network was retrained on the detector-voltage trajectories (Fig. 4e) with ten groups per concentration for training and ten for validation, and only two groups were reported as outside the tolerance, giving 96 % [10]. Because Fig. 4a labels the network as deep learning for classification and Fig. 3i tallies predictions by concentration level, it appears to assign each measurement to one of the five calibrated levels rather than to regress a continuous value, so the quoted accuracy is a class-assignment rate at 0.5 mg/mL spacing and not a measurement resolution (this reading is the reviewer's).

3. Validation Practice

Repeated measurements from the same suspension are strongly correlated, so a random split of replicates can leak information between training and test sets and inflate accuracy [14]. The reviewed microplastic studies split replicates rather than independent preparations, report no comparison with simpler baselines such as linear or partial-least-squares regression, and train on a single polymer and size. The high accuracies should therefore be read as evidence of repeatability, not of generalisation.

4. K-Nearest-Neighbours Classification of Particle Type

In [11] the classifier operates on a four-dimensional feature vector, the frequency shift and S21 amplitude change at the two resonances (about 1.2 and 2 GHz), and was trained on 50 measurements for each of four materials: polyethylene, polystyrene (PS), soda-lime glass and brine-shrimp eggs. On 10 test measurements per material it classified polyethylene and eggs 10/10, glass 9/10 and polystyrene 8/10, an overall 37/40 or 92.5 % (reviewer's calculation) [11]. Two points qualify the claim of polymer identification: only two true polymers were tested, and particle size is not sensed but imposed by a five-stage sieve stack, which retained 2–10 % of 165–300 µm particles on the 300 µm sieve depending on the material (10, 17, 28 and 48 of 500 for polyethylene, eggs, glass and polystyrene) [11].

Table 1: Comparison of Representative Microwave Microplastic Sensing Studies

Author, year	Objective	Sensing / method	Major reported findings	Limitations
Malyuskin, 2020 [6]	Feasibility and theory for soil and water	Capacitively loaded PCB ring, S_{11} at ~5.5 GHz; Nylon 11, 50 µm–0.5 mm	Linear Δf vs concentration model matches data; theoretical resolution ≈ 100 ppm; Δf ≈ 45–65 MHz at 500 ppt in soil and > 140 MHz in water	High concentrations (tens to hundreds of parts per thousand); one polymer; Q falls ≥ 5× if fully immersed; preliminary water data
Desbas, 2024 [13]	Detect microplastics in water with low-cost PCB resonators	Two interdigital resonators with microchannel; VNA 1–6 GHz; sanded bottles, tyre rubber	Max shift 525 MHz (design 1) and 105 MHz (design 2) as stated in the abstract; Q 74–99; 0.1–1 %, < 300–75 µm; only ~6 MHz between concentrations (< 300 µm)	Distilled water only; tap-water constituents not isolated; responses converge for ≤ 150 µm; abstract shifts differ from Table 4.1
ShafieiDarabi, 2025 [11]	Exploratory microfluidic sensing	Microfluidic resonator; PE microspheres 20 and 70 µm	Shift depends on size, concentration and temperature; trends agree with simulation; LoD 10^6 (70 µm) and 10^7 (20 µm) particles/L	Shifts smaller than simulated (≈ 0.5 vs 4 MHz); detection limit above typical freshwater levels
ShafieiDarabi et al., 2025 [12]	Size and concentration characterisation	Coupled IDC + SRR; 20, 70, 275 µm; 10^5–10^7 particles/L	Size and concentration monitored accurately	Fixed microlitre volumes; no continuous flow

Author, year	Objective	Sensing / method	Major reported findings	Limitations
ShafieiDarabi, 2025 [11]	Size, type, concentration	Microfluidic single-particle sensing; KNN on raw data; 20–300 µm	Joint size, polymer and concentration estimation; type accuracy 80–100 % (92.5 % overall)	Size set by sieving, not sensed; only PE and PS among polymers; 15–35 % of particles missed
Hou et al., 2026 [10]	Real-time seawater monitoring	Ring resonator (~2.8 GHz), tubular PDMS channel, CNN; PVC 6.5 µm, 0.5–2.5 mg/mL	LoD 48.72 ng/mL; response 237 ms; 96–98 % within ±0.01 mg/mL; portable BLE prototype	Filtered seawater; replicate split; one polymer for CNN; temperature and salinity compensation needed; stated tolerance inconsistent with Fig. 4g

Table 2: Sensor Platforms, Substrates and Reported Quality Factors

Study	Substrate and fabrication	Topology and operating band	Quality factor (Q)	Readout and sample handling
Malyuskin, 2020 [6]	FR4, 1.6 mm; printed circuit; acrylic sample holder (12 × 12 × 10 mm)	Capacitively loaded square ring (d = 12 mm); gap 0.5–3 mm gives 5.40–6.10 GHz (simulated); S_{11}	Simulated 87–223 (223.1 at 0.5 mm gap); measured 119.4 (air), 259.8 (sand), 92.4 (topsoil), 157.4 (Nylon 11); water cell: 218.7 (air), ≈ 110 (tap), 101.5 (salty)	Keysight E8361C network analyser; static soil holder; 1 mm × 9 mm water mini-channel with syringe pump
Desbas, 2024 [13]	Rogers RT/duroid 5880 (ε_r 2.2, tan δ 0.0009), 1.6 mm; photosensitive-ink etching; PDMS (Sylgard 184) channel from a 3D-printed ceramic mould	Two interdigital microstrip resonators, 1–6 GHz; unloaded 3.51 and 4.17 GHz (sensor 1), 2.34 and 2.84 GHz (sensor 2)	74.11 to 99.14 (sensor 1, unloaded to loaded); 69.20 to 73.75 (sensor 2)	VNA, 801-point sweep; syringe pump; sensor 2 needed an open container
ShafieiDarabi, 2025 [11] (exploratory)	PDMS replaceable reservoir bonded by oxygen plasma; substrate not stated in the sections reviewed	SRR with 1 mm capacitive gap; S_{11}	Not stated in the sections reviewed	Anritsu MS2028C (100 kHz resolution); 10–30 °C chamber; 0.1 % Tween 20 background
ShafieiDarabi et al., 2025 [11], [12]	Planar reader with SRR tag; disposable reservoir holder	Interdigital capacitor plus SRR, tag–reader coupling	Not stated in the sections reviewed	Fixed microlitre volumes; multiplex testing

Study	Substrate and fabrication	Topology and operating band	Quality factor (Q)	Readout and sample handling
ShafieiDarabi, 2025 [11] (single particle)	Planar reader with two SRRs on Wilkinson power dividers; disposable PDMS chip	Two resonances, 1.227 and 2.617 GHz (simulated); channel width matched to SRR gap	Not stated in the sections reviewed	50 µL/min; reading every 500 ms; five-stage sieve pre-filtering
Hou et al., 2026 [10]	Taconic TLX-8 (ε_r 2.55, tan δ 0.0019), 0.508 mm; photolithography and etching; PDMS 1:10 from a 3D-printed mould	Ring-type resonator, S_{21}; simulated 2.8 GHz (−48.5 dB); loaded 1.89–2.05 GHz (Fig. 2)	≈ 21–27 (read from Fig. 2; falls with concentration)	VNA for training data; VCO, power detector, microcontroller and BLE in the portable unit; 20 µL, peristaltic pump

Table 3: Dielectric Properties Used or Measured in the Reviewed Studies

Material	Real permittivity ε′	Loss tangent	Frequency or condition	Source
Fresh (tap) water	72.0 ± 0.50	0.28 ± 0.02	5.5 GHz, 20 °C	Malyuskin [6] (literature values)
Salty water (30 ppt)	66.0 ± 0.40	0.80 ± 0.07	5.5 GHz, 20 °C	Malyuskin [6] (literature values)
Water (general)	≈ 80	—	Microwave band, typical	ShafieiDarabi [11]
Topsoil, dry	4.70 ± 0.20	0.03 ± 0.002	5.5 GHz, measured	Malyuskin [6]
Sandy soil, dry	5.60 ± 0.20	0.007 ± 0.002	5.5 GHz, measured	Malyuskin [6]
Nylon 11 powder	2.59 ± 0.20	0.008 ± 0.002	5.5 GHz, measured	Malyuskin [6]
Polyethylene particles	≈ 2.4	—	Sensing band 1–3 GHz	ShafieiDarabi [11]
Plastic inclusion in Maxwell-Garnett model	2.25	—	Model input	Desbas [13]
Microplastics (typical range)	≈ 2–3.5	—	—	ShafieiDarabi [11]
Wet sediments; blood	10–30; 50–60	—	—	ShafieiDarabi [11]
Rogers RT/duroid 5880 substrate	2.2	0.0009	Substrate, as stated by authors	Desbas [13]
Taconic TLX-8 substrate	2.55	0.0019	Substrate, as stated by authors	Hou et al. [10]

VI. Portable System and Iot Integration

Benchtop VNAs are the main barrier to field use. Hou et al. replaced the VNA by a voltage-controlled oscillator (VCO) and a power detector: a digital potentiometer (X9C503S) sets the tuning voltage, the detector output is digitised by the 12-bit analogue-to-digital converter (ADC) of an STM32F103RET6 microcontroller, and a Bluetooth Low Energy (BLE) 5.2 module sends data to a mobile device for CNN inference and display [10]. In concentration mode the system runs at a fixed 2.8 GHz excitation while monitoring the detector voltage during continuous flow, with a settling time below 250 ms; its output agreed closely with the VNA for blank seawater and a 0.05 % sample [10]. The thesis literature stops at bench measurements with VNAs [11], [13].

The prototype board measures roughly 13 × 10 cm (Fig. 5a of [10]); the text gives the tuning supply as 30 V in the hardware description but as 18 V in the Methods and in Fig. 4a, which should be reconciled. Loading and unloading settle in under 250 ms, comparable with the 237 ms response time of the sensor itself [10]. The signal left for the classifier is small: in Fig. 4e the detector output drops from about 1.4 V to about 0.8 V on loading, but the plateaus for the five concentrations lie at roughly 0.799, 0.805, 0.811, 0.815 and 0.819 V, steps of 4–6 mV, labelled 0.05–0.25 % (equivalent to 0.5–2.5 mg/mL if the percentages are weight/volume). With a 12-bit converter referenced to a few volts such a step is only a handful of counts, so noise, supply drift and temperature are likely to matter (reviewer's estimate).

Compared with the milk and food sensing systems, which already run models on edge boards and forward results over message queuing telemetry transport (MQTT) or narrowband IoT (NB-IoT), the microplastic prototype is at an early stage: inference runs on the receiving device, no long-term field deployment is reported, and a 3-week stability test is the longest operation described [10].

VII. Comparative Analysis

Table I summarises representative studies. Findings fall into a consistent pattern: all resonator designs detect microplastics through frequency shift, but sensitivity depends strongly on particle size, concentration, matrix and where particles sit in the field. Reported figures are not directly comparable because concentrations are expressed as parts per thousand (ppt) or parts per million (ppm) of volume [6], percentage [13], particles/L [12] and mg/mL [10]; and because the 48.72 ng/mL detection limit [10] lies far below the 0.5–2.5 mg/mL range actually calibrated.

Sensitivity can be compared more fairly through the slope of resonance shift against concentration, although the units differ. In [10] the fitted slopes are −0.015, −0.014 and −0.0064 GHz per mg/mL in deionised water, artificial seawater and natural seawater, with coefficients of determination (R2) of 0.971, 0.910 and 0.938, so the response in natural seawater is less than half that in deionised water, and the whole 0.5–2.5 mg/mL range spans only about 13 MHz near 1.9 GHz (calculated from the reported slopes). The quality factors read from Fig. 2 of [10] are about 21–27, several times below the 69–99 of Desbas [13] and the 92–260 measured by Malyuskin [6]; a low Q broadens the resonance and may help explain why a neural network was preferred to simple peak tracking. Particle size is also handled very differently: 6.5–25 µm PVC at mass concentrations in [10], 20–300 µm spheres counted per litre in [11], and 50 µm–0.5 mm or 75–300 µm particles in [6] and [13], so even the size ranges barely overlap.

Three consistency checks suggest that the headline figures of [10] should be treated as provisional until the authors' data are available. First, if the limit of detection LoD = 3S0/S uses the frequency calibration slope (the article does not say which response was used), 48.72 ng/mL implies a standard deviation S0 of only about 0.1–0.24 kHz for slopes of 6.4–15 MHz per mg/mL, hundreds of times finer than the 100 kHz resolution of the analyser in [11]. Second, the limit lies about four orders of

International Journal of Statistics and Mathematical Research Trends
E-ISSN: 3108-0871, Volume 2 Issue 5
Sep-Oct 2026, PP 01-13

magnitude below the lowest calibrated concentration, so it is an extrapolation; with an assumed PVC density of about 1.4 g/cm3 (not stated in [10]) it corresponds to roughly 0.03 ppm by volume, about three orders of magnitude below the 100 ppm linear-regime bound that Malyuskin derives for Q up to 2500 [6], and although the two bounds belong to different sensors and receivers, the gap shows why independent confirmation is needed. Third, the stated tolerance of ±0.01 mg/mL is hard to reconcile with the predictions printed in Fig. 4g of [10], which differ from the true concentration by up to about 0.09 mg/mL for groups counted as correct and by about 0.11–0.13 mg/mL for the two flagged failures, values more consistent with a tolerance near ±0.1 mg/mL. Smaller inconsistencies exist elsewhere: [10] quotes R2 > 0.96 for artificial seawater while Fig. 2II(c) shows 0.9103, and the abstract of [13] gives maximum shifts of 525 and 105 MHz while its Table 4.1 lists first-generation shifts of 56 and 163 MHz (sensor 1) and 30 and 806 MHz (sensor 2). These may be typographical, but they should be resolved before the numbers are reused.

VIII. Proposed Conceptual Architecture

Fig. 1 presents a conceptual seven-layer architecture derived from the reviewed systems. Water is sampled from rivers, treatment plants or points of use (layer 1) and conditioned by size pre-filtering, dispersion, temperature and salinity sensing and a particle-free baseline reading of the same water (layer 2) [11], because matrix effects and particle aggregation dominate the reported errors [6], [10]. The microwave-microfluidic sensor, with a pump, planar resonator and VCO-based readout, measures under continuous flow (layer 3). An embedded unit digitises, normalises and corrects the signal for temperature and salinity (layer 4). Edge models estimate concentration, classify polymer and size, and output a confidence score and anomaly flag (layer 5) [10], [11]. Results are sent by BLE, MQTT or a low-power wide-area link to a dashboard with alerts (layer 6). A sampled subset is verified by laboratory FTIR or Raman analysis and models are retrained only after independent, grouped re-testing (layer 7), addressing the calibration dependence and leakage concerns noted above [3], [4], [14].

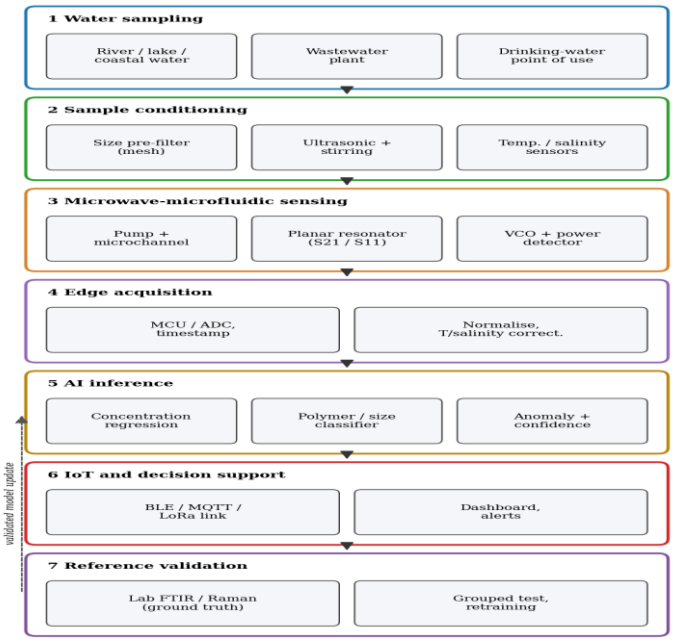


Fig. 1. Proposed conceptual architecture for microwave sensor-based microplastic monitoring from sampling to validation (conceptual, not experimentally validated).

Research Gaps and Future Directions

Gaps supported by the reviewed evidence. (i) Limited matrices: natural seawater was filtered and tap water was not characterised [10], [13]. (ii) Narrow materials: the CNN work used 6.5 µm PVC only, while particle shape, additives and biofouling are not studied [10]. (iii) Concentration mismatch: calibration spans mg/mL, tens of ppt or percentage levels, whereas detection limits are quoted in ng/mL or ppm and environmental levels are far lower [6], [10], [11]. (iv) Weak validation: random splits of correlated replicates and no simple-model baselines [10], [14]. (v) Environmental drift: temperature and salinity shift all resonance parameters and need active compensation [10]. (vi) No common reporting unit or standard protocol, which prevents comparison between sensors. (vii) Little evidence of field operation, fouling, or calibration life beyond three weeks [10]. (viii) Inconsistent sign and size of the response: the resonance moves upward in [6], [11], downward in [10] and in both directions in [13], and the shift across the tested range varies from about 0.5 MHz at 107 particles/L [11] to about 13 MHz over 2 mg/mL in natural seawater [10]. (ix) Instrument limits: analyser resolution (100 kHz in [11]; 801-point sweeps in [13]) bounds the achievable detection limit, and the limit of detection in [10] cannot be reproduced from the information given. (x) Dependence on pre-processing: size is imposed by sieving and filtration [10], [11], and sieve clogging and material-dependent sorting efficiency alter results [11]. (xi) Single-particle reliability: 15–35 % of particles were missed at 50 µL/min [11]. (xii) Ambiguous accuracy metrics: the tolerance and the classification-versus-regression question in [10]. (xiii) Carrier-liquid permittivity: low-molarity salts and urea change the baseline [11].

Directions requiring investigation. Priorities include multi-polymer, multi-size datasets with laboratory reference labels from FTIR or Raman; unfiltered natural-water trials with drift and temperature compensation; higher-Q or differential resonator arrays and low-noise readout to approach the theoretical resolution limit [6]; grouped validation and uncertainty-aware or out-of-distribution detection at the edge; on-device inference with long-term IoT operation; and a shared concentration-reporting standard. The theses add specific recommendations: pre-concentration by on-site filtration or on-chip particle capture followed by flow-through detection; matching the resonator gap or channel width to the particle size; arrays of sensors tuned to particular sizes or polymers; flow control that keeps particles in the sensing region longer; funnel-based or vertical-pump sample entry to avoid deposition in the syringe; microfluidic pre-sorting more reliable than sieves; adjusting the dielectric contrast of the carrier; and a higher-resolution analyser, for which the 200,000-point Copper Mountain M5090 is proposed [11]. Desbas recommends field tests with environmental samples and integration into portable in-line monitors [13].

IX. Conclusion

Microwave resonator sensing has progressed from a feasibility demonstration in soil and water [6], through PCB and microfluidic sensors that detect and size particles [11]–[13], to a portable, Bluetooth-enabled seawater prototype with CNN-based concentration estimation [10]. Reported performance is encouraging: shifts of hundreds of MHz, response times of a few hundred milliseconds, and accuracies of 96–98 % under controlled conditions. The evidence base is, however, dominated by laboratory studies with filtered or artificial matrices, a few polymers, non-standard units and weak validation. Quality factors range from about 21 to 260 and particle sizes from 6.5 µm to 0.5 mm across the studies, and several headline figures of the seawater study (the 48.72 ng/mL limit of detection and the ±0.01 mg/mL tolerance) could not be reconciled with the data shown, so they should be regarded as provisional. Reliable deployment will require realistic matrices, multi-polymer datasets, environmental compensation, grouped validation and continuous reference-based model maintenance, as reflected in the proposed architecture. Microwave sensors are therefore best viewed as a low-cost screening tool that complements, rather than replaces, FTIR and Raman analysis.

References

1. R. C. Thompson et al., “Lost at sea: Where is all the plastic?,” Science, vol. 304, no. 5672, p. 838, 2004.

2. H. A. Leslie et al., “Discovery and quantification of plastic particle pollution in human blood,” Environ. Int., vol. 163, Art. no. 107199, 2022.
3. X. Yan, Z. Cao, A. Murphy, and Y. Qiao, “An ensemble machine learning method for microplastics identification with FTIR spectrum,” J. Environ. Chem. Eng., vol. 10, 2022.
4. C. Fang, O. S. Awoyemi, Y. Luo, and R. Naidu, “How to identify and quantify microplastics and nanoplastics using Raman imaging?,” Anal. Chem., vol. 96, pp. 7323–7331, 2024.
5. D. M. Pozar, Microwave Engineering, 4th ed. Hoboken, NJ, USA: Wiley, 2011.
6. O. Malyuskin, “Microplastic detection in soil and water using resonance microwave spectroscopy: A feasibility study,” IEEE Sensors J., vol. 20, pp. 14817–14826, 2020, arXiv:2004.08713.
7. K. H. Lee, J. H. Kim, K. S. Shin, C. U. Cha, and H. M. Lee, “Complementary multisplit ring resonant MEMS sensor with microfilter for microplastics concentration measurement,” IEEE Sensors J., vol. 23, pp. 19105–19116, 2023.
8. P. Zhao et al., “Detection of microplastics by microfluidic microwave sensing: An exploratory study,” Sens. Actuators A, Phys., vol. 383, 2025.
9. Y. C. Alatas, U. Tefek, S. Salehin, H. Alhmoud, and M. S. Hanay, “Rapid differentiation between microplastic particles using integrated microwave cytometry with 3D electrodes,” ACS Sens., vol. 10, pp. 1729–1735, 2025.
10. Y. Hou et al., “Portable microwave sensor system for real-time detection of microplastics in seawater,” Microsyst. Nanoeng., vol. 12, Art. no. 302, 2026, doi: 10.1038/s41378-026-01413-y.
11. S. M. ShafieiDarabi, “Development of microwave-microfluidic sensors for microplastic detection in environmental samples,” Ph.D. dissertation, Dept. Mech. Mechatronics Eng., Univ. of Waterloo, Waterloo, ON, Canada, 2025.
12. M. ShafieiDarabi, Z. Abbasi, and C. L. Ren, “Size and concentration characterization of microplastic particles in aqueous samples using sensitivity-enhanced coupled planar microwave resonators,” J. Hazard. Mater., vol. 495, 2025.
13. J. Desbas, “Low-cost microwave sensor for detecting the first generation of microplastic in aqueous media,” M.Sc. dissertation, Dept. Elect. Eng., Univ. of Brasília, Brasília, Brazil, 2024.
14. S. Kapoor and A. Narayanan, “Leakage and the reproducibility crisis in machine-learning-based science,” Patterns, vol. 4, no. 9, Art. no. 100804, 2023, doi: 10.1016/j.patter.2023.100804.